We are IntechOpen, the world's leading publisher of Open Access books
Built by scientists, for scientists

6,900
Open access books available

186,000
International authors and editors

200M
Downloads

Our authors are among the

154
Countries delivered to

TOP 1%
most cited scientists

12.2%
Contributors from top 500 universities

CLARIVATE ANALYTICS
BOOK CITATION INDEX
INDEXED

WEB OF SCIENCE™

Selection of our books indexed in the Book Citation Index
in Web of Science™ Core Collection (BKCI)

Interested in publishing with us?
Contact book.department@intechopen.com

Numbers displayed above are based on latest data collected.
For more information visit www.intechopen.com

Measuring Nanofluid Thermal Diffusivity and Thermal Effusivity: The Reliability of the Photopyroelectric Technique

Monir Noroozi and Azmi Zakaria

Additional information is available at the end of the chapter

Abstract

It is important to study nanofluids to understand their extraordinary thermal properties and how the size, concentration and agglomeration of the nanoparticles affect those properties. Photopyroelectric (PPE) technique has been well established in the use of non-destructive measurement of thermal diffusivity and thermal effusivity, by using polyvinylidene fluoride (PVDF) films as sensitive pyroelectric sensors in thermally thick conditions instead of using very thick ceramic sensors. There have been two proposed practical configurations for the PPE technique, the back and the front PPE configurations, to obtain both the thermal diffusivity and effusivity, which are suitable thermal parameters of materials. This PPE technique involves the measurement of thermal waves in the sample due to absorption of optical radiation, by placing a pyroelectric sensor in thermal contact with the sample. This chapter provides a review of the back and the front PPE configurations to determine the thermal diffusivity and effusivity of nanofluids, sample preparation techniques using high-amplitude ultrasonic dispersion and data analysis for metal oxide-based nanofluid materials.

Keywords: nanofluids, thermal properties, photopyroelectric technique, thermal diffusivity, thermal effusivity

1. Introduction

Water, ethylene glycol (EG) and oil are universally used for transfer heating, but unfortunately these fluids have extremely poor thermal conductivity; thus, smaller and lighter heat exchanges could be reduced leading to reduced power and the size of the required heat transfer. As can be seen in **Figure 1**, the thermal conductivity of copper is about 700 times more than the water and about 3000 times more than the engine oil.
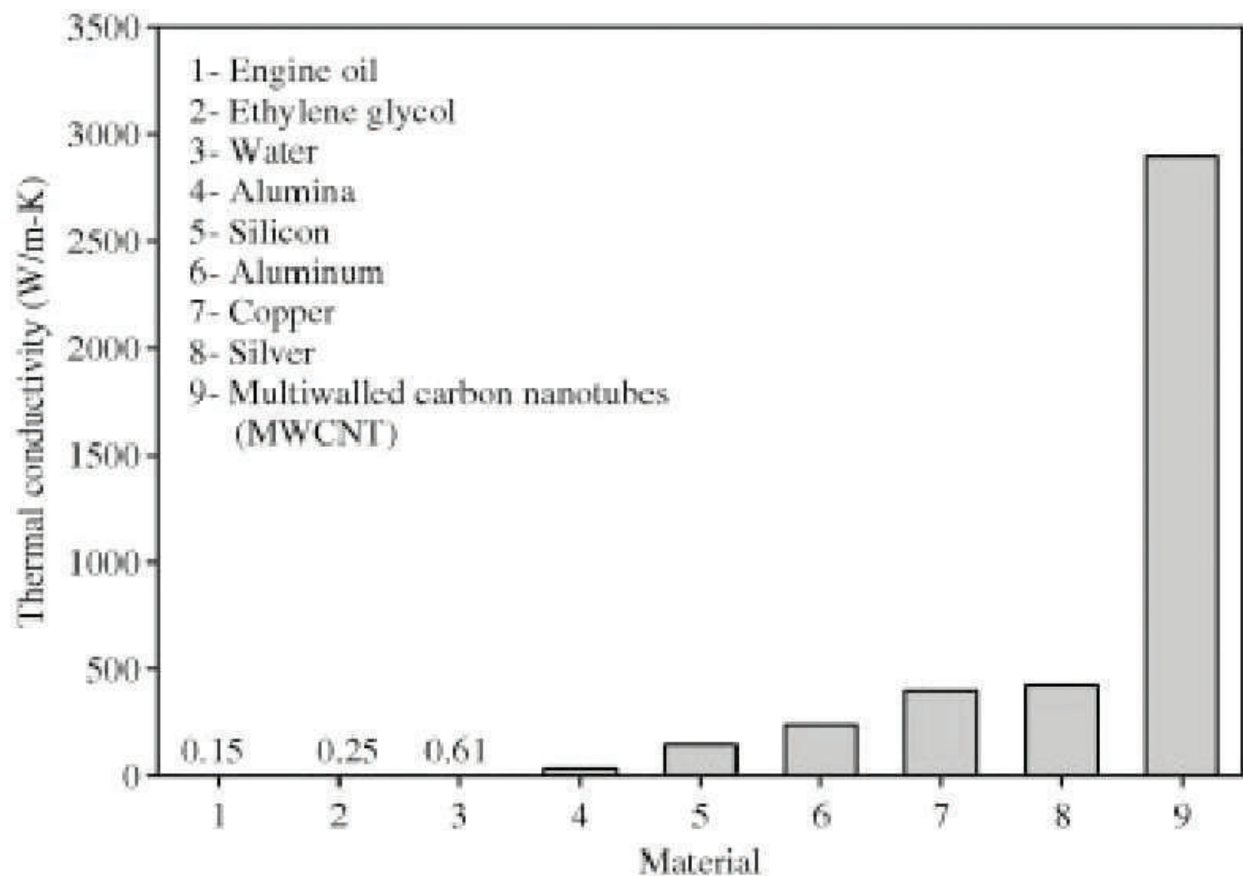
Figure 1. Thermal conductivity of the materials (solids and liquids) at room temperature [1].

The study of heat transport in solid-liquid dispersions (colloids) began as early as in the 1970s. The first thermal conductivity enhancement of nanoparticles (NPs) was reported by Masuda et al. [2]. Due to the size of the NPs, they are well suited for use in microsystems. It was observed that the thermal conductivity of an ultrafine suspension of metal oxides in water increased up to 30% for an NP volume fraction of 4.3%. The term 'nanofluid' was first coined by Choi and Eastman [3] when he reported a class of engineered fluids containing nanosized particles dispersed in ethylene glycol that had a thermal conductivity with almost a factor of 2 greater than the base fluid. Nanofluids have widespread usage in industry, including medicine applications, engineering applications, in cooling/heating systems and in micromechanical systems, due to their enhanced thermal management. Nanofluids are able to improve heat transfer and, thus, allow for smaller pumping, heaters and other elements. Nanofluids containing metals and metal oxides have been considered as the next generation of the heat transfer fluids, as they have shown an increase in their effective thermal conductivity compared to their base fluid [4]. Metal oxide nanofluids have potential applications in the main processing industries, such as the materials, chemistry, biomedicine, food and drink, oil and gas industries as they are able to enhance thermal transfer [4, 5].

The preparation of nanofluids is an important parameter in the investigation of the thermal properties of nanofluids. Nanofluids can be prepared by directly dispersed nanopowders in

the base fluid, but this method could result in a large degree of NP agglomeration. Therefore, a clear understanding of the effect of concentration, dispersion/aggregation state and particle size on the thermal properties of prepared nanofluid is an essential assay step for particle validation. Data has shown that the thermal conductivity of nanofluids could significantly be increased with an increase in the volume fraction of NPs [6–8]. It is clear that four thermal parameters can be connected by two relationships, $\alpha = k/\rho C$ and $(e = k/\sqrt{\alpha})$, where C, α, k and e are the volume specific heat, thermal diffusivity, conductivity and effusivity, respectively. Although the thermophysical properties of nanofluids are intensely researched at present, most of the studies have been focused on measuring the thermal conductivity of the nanofluids.

There are only a few reports on the thermal diffusivity measurements using thermal lens spectrometry and the transient double-hot-wire method [9]. However, these methods often require high temperatures to obtain reasonable signal-to-noise (SNR) ratios, which in turn, could increase the sample temperature and thus increase the measurement error. These techniques are also disadvantageous because they require high-volume samples, long measurement times without according the effect of aggregation time and are expensive. Nowadays, highly sensitive photopyroelectric (PPE) techniques have been designed to measure the thermal properties of samples and are actually one of the several available photothermal techniques [10–12]. The thermal parameters directly resulting from the PPE experiment are usually the 'fundamental' ones: the thermal diffusivity and also the thermal effusivity. The unique features of the back and front PPE techniques to measure the thermal diffusivity and the thermal effusivity of nanofluids in high resolution are that they are not possible with other existing techniques [13]. The advantages of this method include its relatively low cost, and only a small volume of the sample is required with a short measurement time, where the concentration of the nanofluid remains constant in the measurement process, thus making this technique suitable for nanofluids. In the principle by using both the back PPE and front PPE configurations, source of information (amplitude and phase of pyroelectric signal), cavity scanning or frequency scanning, it is possible to obtain both the thermal diffusivity and thermal effusivity. Recently, a new simplified front PPE configuration was designed using a metalized polyvinylidene fluoride (PVDF) sensor in a thermally thick condition instead of using the very thick ceramic sensors of typically 300 μm [14] or 500 μm in size [15] (usually $LiTaO_3$) that have to be coated with gold with a very low chopping frequency facility.

The present chapter provides a review on the thermal properties of nanofluids measured by the PPE technique by using frequency scans of the signals employing PVDF as a pyroelectric (PE) sensor in thermally thick conditions, due to its low cost, light weight, flexibility and sensitivity. The back and front PPE configurations in 'thermally thick' conditions have been implemented to measure the thermal diffusivity and the thermal effusivity of nanofluids (containing Al_2O_3 and CuO NPs) as a function of the base fluid's particle size. To reduce agglomeration of the NPs, an ultrasonic dispersion technique was utilized for in low concentration of the NPs to produce stable nanofluids, and the effects of sonication type on the stability and thermal properties were investigated.

2. Thermal properties of the nanofluids

2.1. Synthesis and stability of nanofluids

The preparation of nanofluids is an important parameter in the investigation of the thermal properties of nanofluids. The preparation of nanofluid is not merely a simple mixing of liquid and nanopowder, and thus a good dispersion method of dispersing NPs in liquids or a direct production of stable nanofluids is crucial. A good dispersion of NP materials into liquids such as deionized water (DW), ethylene glycol (EG) or oil is needed for producing a stable nanofluid. There are primarily two methods for the synthesis of nanofluids, including the two-step process and the single-step process for the direct synthesis of nanofluids.

The two-step method is achieved by firstly synthesizing dry NPs with the preferred size and shape. In the second step, these particles are carefully mixed into the required base fluid in the desired volume fraction, typically with some additives to enhance the stability of the nanofluids. Thus, the small volume fraction of NPs and proper dispersion techniques are important for the preparation of stabile nanofluids in this technique. Many researchers have reported successful fabrication and testing of nanofluids using the two-step preparation method [16, 17]. Due to the high surface area of the NPs, they have the tendency to aggregate. A large degree of agglomeration in NPs may occur as a result of using this method. Thus, proper dispersion techniques, such as the ultrasonic dispersion technique [18] or the fragmentation process of NPs using laser irradiation, in low concentrations of NPs, are important for the production stability of nanofluids. Another technique to enhance the stability of NPs in fluids is the use of surfactants. To summarize, the optimization of thermal characteristics of nanofluids requires stable nanofluids, which can be achieved by synthesis and dispersion processes.

2.2. Experimental investigation methods

2.2.1. Thermal diffusivity measurement techniques

Highly sensitive photothermal methods using a laser as an optical source have been widely used in the thermal diffusivity measurements of nanofluids [19–28]. The photothermal effect in a material is a consequence of the deposition of heat in the sample following absorption of a laser beam and subsequent thermal de-excitations, which results in the indirect heating of the sample. Photoacoustics, photothermal deflection, thermal lens, photothermal radiometry and photopyroelectric methods are some of the techniques commonly used powerful for thermal and optical characterization of materials using lasers. The conventional techniques such as the 'hot-wire', 'laser flash', '3ω-wire method' and 'optical (forced Rayleigh light scattering)' techniques have also been utilized by some researchers [29–33], as seen in **Table 1**.

2.2.2. Thermal effusivity measurement techniques

Very few studies have been reported on the determination of the thermal effusivity of liquids. During the last two decades, the front PPE configuration and photoacoustic techniques have been used for determining the thermal effusivity [13–15]. For the front detection configuration,

References	Particle type	Base fluid	Particle fraction	Enhancement	Method
Dadarlat et al. [19]	Fe_3O_4	Transformer oil	0–623 mg/ml	$(9.06–9.84)\ 10^{-8}\ m^2/s$	Thermal-wave resonator cavity
Nisha and Philip [20]	TiO_2/PVA 5–100 nm	Water	(1–5)vol%	Increases at high concentrations and high particle size	Thermal-wave interference
Philip and Nisha [21]	TiO_2/PVA	Water	(0.005–0.039) vol%	Normalized thermal diffusivity from 1 to 0.96	Thermal-wave resonator cavity
López-Muñoz et al. [22]	Urchin-like colloidal gold	Water	(0.2–1)wt%	1.02–1.05	Photopyroelectric
		EG	(0.2–1)wt%	1.06–1.11	
		Ethanol	(0.2–1)wt%	1.09–1.14	
Dadarlat et al. [23]	Fe_3O_4	Water	(8.2–81.7) mg/cm^3	High-accuracy results (within ±0.5%). Thermal diffusivity was sensitive to changes in type and NP concentration	Photopyroelectric
	$CoFe_2O_4$	Water	(6.1–24.5) mg/cm^3		
Agresti et al. [24]	Al_2O_3 20–70°C	Water, EG	1 and 2 wt%	For both water and glycol from 1.04 to 1.12	Photoacoustic
López-Muñoz et al. [22]	Gold	Water	(0.2–1)wt%	1.01–1.04	Photoacoustic
Sánchez-Ramírez et al. [25]	Au/Pd	Water	Au/Pd = 12/1, 5/1, 1/1, 1/5	The maximum diffusivity was achieved for the nanoparticles with highest Au/Pd molar ratio	Thermal lens technique
Kumar et al. [26]	Gold 30–50 nm	Water	1% wt	The value decreases with decrease in particle size	Thermal lens technique
Jiménez Pérez et al. [27]	Gold	Water, ethanol and EG	0.1 g/L	Enhanced	Thermal lens technique
Gutierrez Fuentes et al. [28]	Au/Ag nanoparticles	Water	Au/Ag = 3/1, 1/1, 1/3, 1/6	A lineal increment of the thermal diffusivity when the Ag shell thickness is increased	Thermal lens technique
Filippo et al. [29]	Ag	Deionized water	4 vol%	12%	Laser flash
Wang et al. [30]	TiO_2	Water	(1–4)vol% 20–70°C	Vary significantly with temperature An enhancement of up to 19.6% is observed at 4% and 65oc	3ω-Method
	SiO_2	Water, ethanol and EG	(1–4)vol% 20–70°C		
Faris Mohammed and Yunus [31]	Al	Distilled water, ethanol and EG	Five different volume fractions of nanoparticle	Thermal diffusivity increased linearly with increasing concentration of nanoparticles in the respective base fluids	Hot-wire technique
	Al_2O_3				
Murshed et al. [32]	TiO2	EG	(1–5)wt%	1.1–1.3	Hot-wire technique
	Al_2O_3	EG	(1–5)wt%	1.05–1.3	
Rondino et al. [33]	Pyrolytic titania	Ethanol	0.6 vol%	0.6%	Optical technique

Table 1. Summary of experimental studies of thermal diffusivity enhancement.

two schemes were proposed, namely, the configuration with a thermally thin and the optically opaque PVDF sensor [34] and the configuration with a thermally thick and optically semi-transparent sensor using LiTaO$_3$ [15]. Balderas-López et al. [35] applied the front PE configuration to perform high precision measurements of thermal effusivity in transparent liquids in a very thermally thick regime.

Esquef et al. [36], in 2006, developed a method consisting essentially of a photoacoustic cell and a PE cell enclosed in a single compact gas analyzer for the measurement of thermal diffusivity and thermal effusivity. Concerning the front configuration, a simplified method to measure both the thermal diffusivity and thermal effusivity of sensor was proposed. For example, Streza et al., in 2009, [37]applied two PE detection configurations, 'back' and 'front', to the calorimetric studies of some liquids (liquid mixtures, magnetic material nanofluids, liquid foodstuffs, etc.). They demonstrated that if the back configuration used the phase of PE signal in the cavity scan method and the front configuration used the frequency scan, both thermal diffusivity and thermal effusivity could be measured. Dadarlat et al.[23], in 2008, measured the thermal diffusivity and thermal effusivity of Fe$_3$O$_4$ and CoFe$_2$O$_4$ nanofluids by using two PPE detection configurations (back and front). Their thermal diffusivity and effusivity measurements were obtained with high accuracy (within 0.5%), and the results were sensitive to changes in the relevant parameters of the nanofluid as the base fluid, concentration and type of NPs. Thus, the front PPE method [13–15, 35–39] was a suitable for accurate and simultaneous measurements of thermal diffusivity and effusivity of nanofluids.

2.3. Theoretical background: photopyroelectric technique

The photothermal method has been widely used for determining the thermal parameters of materials. This technique typically uses a modulation of laser beam for inducing a thermal-wave (TW) field in the sample. The obtained TW distribution is then detected by various photothermal methods, such as photoacoustics [40], photothermal spectroscopy [41] or PPE techniques [11, 42]. Recently, many useful applications of the photopyroelectric (PPE) effect have been reported with regard to the measurement of both thermal and optical absorption properties of a material [43]. The PPE effect has provided a calorimetric method in which a thin-film PE sensor produces a voltage proportional to its surface temperature change due to the propagation of TWs through a sample in intimate contact with the PVDF sensor. In this technique, the light modulation impinges on the front surface of a sample and the PE sensor, located in good thermal contact with the sample's backside so the PE signal can be measured by performing either a frequency or a cavity length scan. The back and front PPE configurations in 'thermally thick' conditions have been reported to measure the thermal diffusivity and thermal effusivity of a sample [39, 44]. A front PPE technique is the modification of the classical configuration of the PPE technique. In this technique, the TW is introduced to the rear of the PE detection [45]. In the back PPE technique, a very thin metal film is illuminated by a modulated laser beam, and the PE cell consisted of these two parallel walls, one the metallic foil as the TW generator and another the PE film as a PE signal sensor which was placed parallel to the TW generator surface at a fixed cavity length as a function of frequency in frequency scanning and at a given frequency as a function of cavity length in cavity scanning, respectively [46]. This experimental device has allowed the measurement of thermal properties of gas and liquid and liquid mixtures [47]. This expression is typically based on the general theory of PE detection. The experimental results can

then be obtained by using the PPE technique that is designed at different configurations in the measurement of the thermal properties of the nanofluids. The following results and discussion are divided into two parts: (i) the back and (ii) front PPE configurations to measure the thermal diffusivity and thermal effusivity of the nanofluid samples.

2.3.1. Back photopyroelectric theory

In the back PPE technique, named the thermal-wave cavity (TWC) technique, a very thin metal film was illuminated by a modulated laser beam, and the PE cell consisted of these two parallel walls, one the metallic foil as a TW generator and another the PVDF film, as a PE signal sensor. The sample(s) converts the modulated laser beam into TWs.

The induced TWs then transmit through the intracavity medium (l) by TW transmission, and the reflection mechanism is detected by the PE sensor (p), as shown in **Figure 2**. TW's arrival at PVDF film gives rise to the surface temperature at the film ($x = 0$) [48]:

$$\theta_0 = \frac{\theta_{l_s} T_{sl} e^{-\sigma_l l_l}}{1 - R_{ls} R_{lp} e^{-2\sigma_l l_l}} \tag{1}$$

The transmitted terms of TWs, of the solid-liquid interface at ($x = -l$), are given by

$$\theta_{l_s} = \frac{Q_0 T_{gs} e^{-\sigma_s l_s}}{1 - R_{sg} R_{sl} e^{-2\sigma_s l_s}} \tag{2}$$

Hence, the surface temperature of the PVDF can be continued as

$$\theta_0 = \frac{Q_0 T_{gs} T_{sl} e^{-(\sigma_s l_s + \sigma_l l_l)}}{\left(1 - R_{sg} R_{sl} e^{-2\sigma_s l_s}\right)\left(1 - R_{ls} R_{lp} e^{-2\sigma_l l_l}\right)} \tag{3}$$

where Q_o is the TW source intensity, σ_j is the complex TW diffusion coefficient $\sigma_j = (1 + i)/\mu_j$ and T_{jk} and R_{jk} are TW transmission coefficient and TW reflection coefficient, respectively, at (j–k)
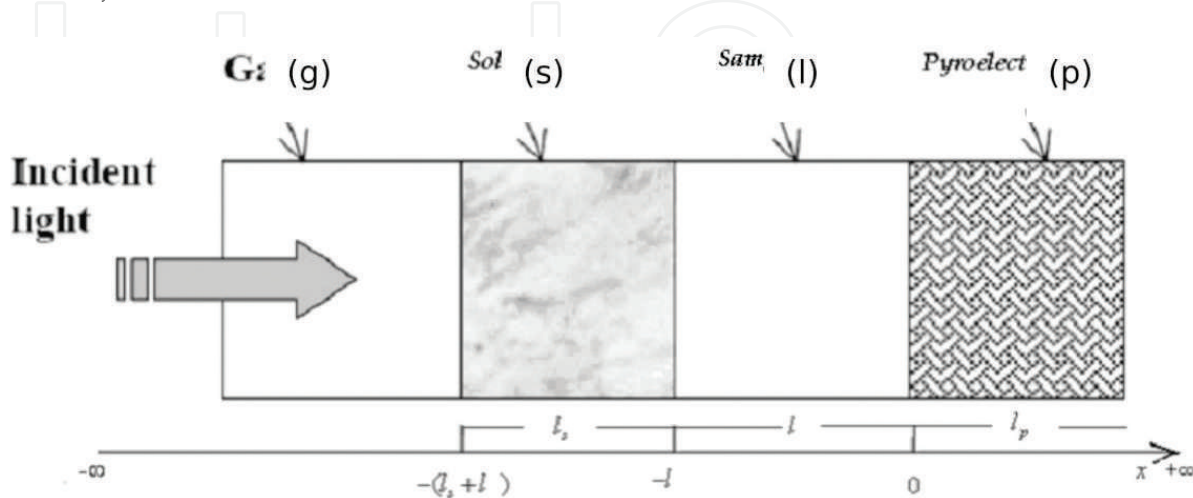

Figure 2. 1D configuration of TWC showed that the thermal waves are partially reflected and transmitted upon striking the boundaries (g, s, l, p and b) which stand for gas, solid, liquid sample, PVDF film and backing, respectively.

interface, defined as $T_{jk} = \frac{2}{1+b_{jk}}$; $\quad\quad R_{jk} = \frac{1-b_{jk}}{1+b_{jk}}$; $\quad\quad b_{jk} = \left(\frac{k_k}{k_j}\right)\left(\frac{\alpha_j}{\alpha_k}\right)^{1/2}$. The following param-
eters were also defined: α_j, the thermal diffusivity of j (= g, s, l, p, b); μ_j (= $(\alpha_j/\pi f)^{1/2}$), the thermal
diffusion length of j at modulation frequency f; and l_j, the thickness of j. The temperature
distribution in PVDF film from two parts, the PVDF film-liquid interface and the PVDF film-
backing interface, can be written as

$$\theta_p(f,x) = \theta_0 \frac{T_{lp}\left(e^{-\sigma_p x} + R_{pb}e^{(-2\sigma_p l_p + \sigma_p x)}\right)}{\left(1 - R_{pb}R_{pl}e^{-2\sigma_p l_p}\right)} \tag{4}$$

The average PE voltage is given by

$$V(f,l_1) = \frac{p}{\varepsilon\varepsilon_o} < \theta_p >= \frac{Q_o T_{sl}T_{lp}pe^{-\sigma_s l_s}\left(1 - e^{-\sigma_p l_p}\right)\left(1 + R_{pb}e^{-\sigma_p l_p}\right)}{\varepsilon\varepsilon_o\sigma_p\left(1 - R_{sg}R_{sl}e^{-2\sigma_s l_s}\right)\left(1 - R_{pb}R_{pl}e^{-2\sigma_p l_p}\right)} \frac{e^{-\sigma_l l_l}}{\left(1 - R_{ls}R_{lp}e^{-2\sigma_l l_l}\right)} \tag{5}$$

If P is the PE coefficient, l_p is the thickness of the PVDF sensor, ε is the dielectric constant of the
pyroelectric sensor, ε_0 is the permittivity constant of vacuum, ω is the angular frequency of
modulated light and R_{jk} is the interfacial thermal coefficients. Considering that for thermally
thick condition $\left|e^{-2\sigma_l l}\right| << 1$, Equation (5) can be written more simply as [49]

$$V(f,L) = \text{Constant } (f)e^{-\sigma L} \tag{6}$$

$$|V(f,L)| = \text{Constant } (f)e^{-L/\mu} \tag{6a}$$

$$\phi(f,L) = \text{Constant } (f) - L/\mu \tag{6b}$$

The thermal diffusivity of sample can be obtained by the slope liner fitting from the plot ln
(amplitude) and phase versus both cavity length (from the cavity scan) and frequency square
(from the frequency scan). In frequency scanning method, the cavity was at a fixed thickness L.
By plotting the phase and ln(amplitude) as a function of frequency scan, the thermal diffusivity
can be determined: $\alpha = \pi L^2 / \left(\frac{\phi}{\sqrt{f}}\right)^2$, $\alpha = \pi L^2 / \left(\frac{\ln(|V|)}{\sqrt{f}}\right)^2$

2.3.2. Front photopyroelectric theory

Usually, the front PPE configuration can be obtained as shown in **Figure 3**, the sensor directly
is irradiated and the sample in contact with its rear surface. Then, the cell structure, gas, PE
sensor and sample, (g/p/s) becomes another variant of PPE technique.

Under this assumption, for a cell structure (g/p/s), the average PE voltage simplifies to [35]

$$V(f,l) = V_s \frac{\left(1 - e^{-\sigma_p l_p}\right)\left(1 - R_{ps}e^{-\sigma_p l_p}\right)}{\left(1 - R_{ps}R_{pg}e^{-2\sigma_p l_p}\right)} \tag{7}$$

where $V_s(f) = P/\varepsilon\varepsilon_o\langle\theta_s\rangle$ with thermally thick sensor and sample, the signal defined by
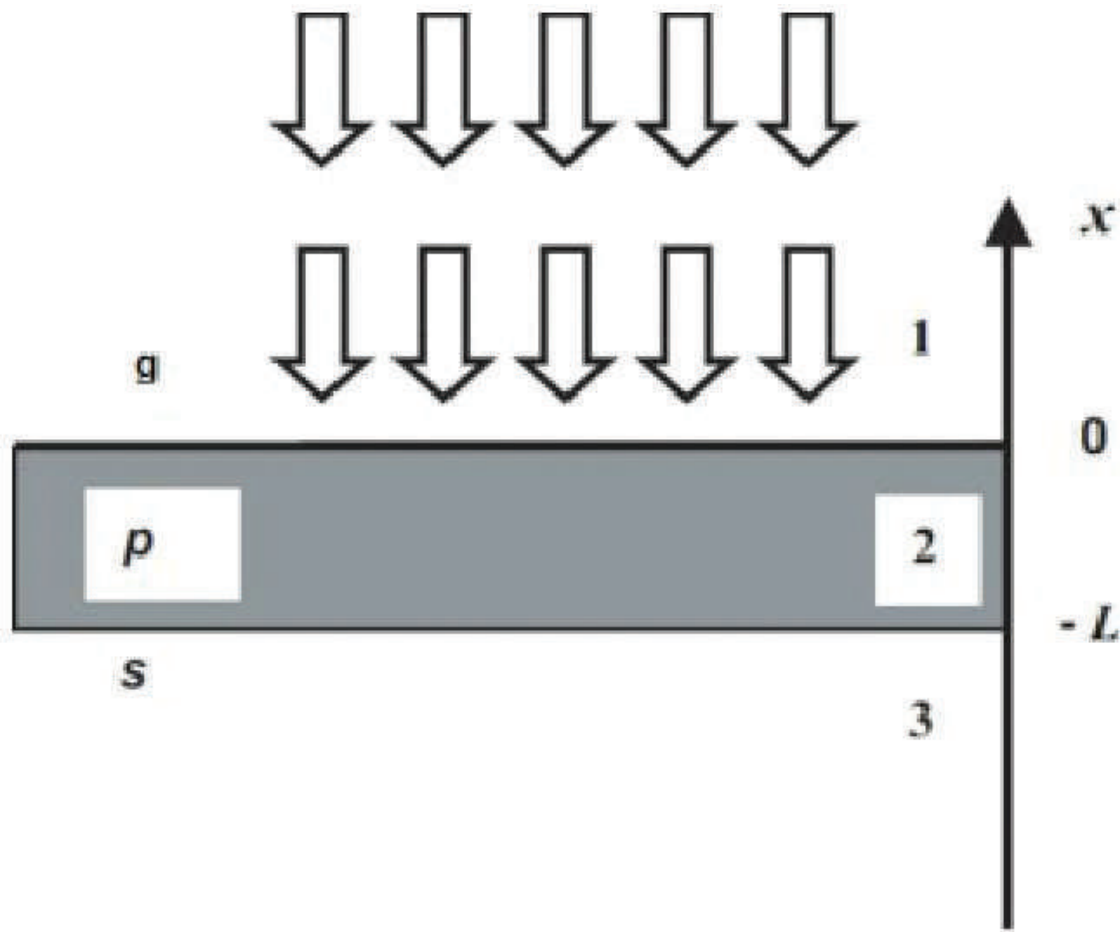
Figure 3. 1D geometry of the front PPE configuration, for a cell structure (g/p/s).

$$V(f) = V_s\left[1-(1+R_{sp})e^{-\sigma_p L_p}\right] \tag{8}$$

$$R_{sp} = (e_s-e_p)/(e_s+e_p) \tag{9}$$

where e_s and e_p are the thermal effusivity of sample and PE sensor, respectively. The normalizing signal is determined (by using air), and the normalized signal becomes

$$V_n(f) = 1-(1+R_{sp})e^{-\sigma_p L_p} \tag{10}$$

The normalized phase and amplitude of the signal are defined by

$$\theta = \arctan\left[\frac{Ae^{-L_p/\mu_p}\sin\left(L_p/\mu_p\right)}{1-Ae^{-L_p/\mu_p}\cos\left(L_p/\mu_p\right)}\right] \tag{10a}$$

$$|V_n(f)| = \left\{\left[A\sin\left(L_p/\mu_p\right)e^{-L_p/\mu_p}\right]^2 + \left[1-A\cos\left(L_p/\mu_p\right)e^{-L_p/\mu_p}\right]^2\right\}^{1/2} \tag{10b}$$

where $A = 1 + R_{sp}$, A the constant can be obtained by optimizing the fit performed on the experimental data with the normalized signal phase by using Equation (10b). It can be shown that from the phase of the normalized signal, one can obtain the thermal effusivity of the liquid sample.

3. Experimental method

3.1. Preparation of metal oxide nanofluids

Nanofluids were prepared by dispersing pre-synthesized NPs into fluids, and if necessary, in the presence of the stabilizer polyvinylpyrrolidone (PVP) to keep the NPs stable in the fluids. Nanopowders into base fluids were dispersed by stirring, and the suspensions were ultrasonicated by using probe-type or bath-type sonicator. Nanofluids were prepared using Al_2O_3 (Nanostructured & Amorphous Materials, Inc.), and copper oxide (Sigma-Aldrich) particles were dispersed in various base fluids, DW and EG. To make the desired volume concentration percentage of NPs in the nanofluids, the weights of the base fluid and NPs were measured using an electric balance (Ohaus Adventurer Balances). For example, 3.97g of Al_2O_3 NPs, which is 1 ml based on the density provided by the vendor, were added to 99g (99 ml) of DW to make 1 % volume concentration of the Al_2O_3/DW nanofluid. All nanofluids are processed by the same ultrasound power.

3.1.1. Ultrasonication dispersion process

Physical dispersion of powders in a liquid can be achieved by ultrasonic irradiation, either in a bath or by direct irradiation using a probe sonication method. Probe sonication has been studied to determine its effect on the particle characteristics such as the average agglomerate size and the surface charges [50]. Probe sonication is expected to provide higher power to the suspension than the ultrasonic bath as the probe is directly immersed in the suspension. The bottles containing the nanofluid were placed in the ultrasonic bath which was filled with water. The influence of the main parameter of ultrasonication such as the irradiation type (probe and bath) to dispersion and reduced size was observed in the suspension of Al_2O_3 in low concentration in water, as shown in **Figure 4**. Al_2O_3 NPs (99%, 11 nm) 0.5 wt% were dissolved in DW and magnetically stirred vigorously until a clear solution was obtained in about 1 h. The suspension was sonicated for 30 min using an ultrasonic probe (VCX 500, 25 kHz, 500 W) and labelled as sample P or using an ultrasonic bath (Powersonic, UB-405, 40 KHz, 350 W), which was labelled as sample B, respectively. As energy transferred into the liquid, the liquid become heated, and a cooling system to control the temperatures between 35 and 40°C was required. This temperature range is favourable to produce a large cavity field that greatly accelerates the integration of NPs in fluids. Unlike the bath sonication that was performed at room temperature, the tip probe sonication had higher amplitudes and, thus, a more effective creation of cavitation and heating. In the case of the ultrasonic probe, the nanoparticle/DW mixture was placed in another larger container filled with ice cubes. This was to prevent the evaporation of fluids caused by elevated temperatures. It was found the

Figure 4. Probe (VCX 500, 20 kHz, 500 W) (*left*) and bath (POWERSONIC, UB-405, 40 KHz, 350 W) (*right*) ultrasonic, respectively.

most appropriate power and conditions were obtained using the ultrasonic probe to achieve the highest dispersion and long-term stability.

3.1.2. Sample characterization

Various techniques have been applied to analyze the chemical and physical properties of the prepared nanofluids. The morphologies of the deposits were studied using an S-4700 field emission scanning electron microscope (FESEM) (Hitachi, Tokyo, Japan), operating at 5.0 kV. The size, distribution and morphology of the synthesized NPs were determined via TEM (H-7100, Hitachi, Tokyo, Japan), and the particle size distributions were determined using the UTHSCSA Image Tool software (version 3.00; UTHSCSA Dental Diagnostic Science, San Antonio, TX). In the characterization of the prepared nanofluids, the particle size and size distribution of spherical NPs in colloidal form were measured by the Nanophox particle size analyzer (Sympatec GmbH System-Partikel-Technik). This equipment is based on the principle of dynamic light scattering, which provides mean particle size as well as particle size distribution (PSD). The surface plasmon or absorption maximum in the colloidal solution spectrum provides information on the average size of the particles, and a UV-Vis spectrophotometer (Shimadzu-UV1650PC) was used to measure the absorption spectra at room temperature for wavelength range 200–800 nm.

3.2. Experimental setup of the photopyroelectric methods

The systematic experiments were to investigate the accuracy of thermal diffusivity and effusivity by the PE method using the back PPE and front PPE configurations as a special

case of the different structures of the PE cell. The basic design of the analytical instrument consisted of only a laser, a TW generator and a PVDF, PE sensor. The thermal diffusivity and thermal effusivity of the nanofluids were obtained with both the back and front PPE configurations.

3.2.1. Back PPE configuration and experimental conditions

The schematic diagram of the experimental setup is shown in **Figure 5**. Here, a 52 µm PVDF film PE sensor (MSI DT1-028K/L), which is an excellent choice for signal detection due to its low cost, low weight, flexibility and sensitivity, was used in signal detection [51]. A 30 mW He-Ne laser (05-HR-991) was modulated by an optical chopper (SR540) before illumination on copper foil of 50µm thickness and 0.8cm diameter. To maximize its optical to thermal conversion efficiency, a very thin layer of carbon soot was coated on the surface of the foil. When the laser was illuminated on the copper foil, TWs were generated in this foil.

In the cell, the initiated TWs propagated across the fluid and reached the PE sensor. Since the PVDF film is very flexible and any film wrap can cause a change of signal, it was fixed with silicon glue to a Perspex substrate. On its top side, a plastic ring of 1 cm diameter was glued to it to act as the sample container. A small volume of the liquid sample, <0.1 cm^3, was simply filled in the inner side of the ring, with a sample depth or thickness of around 1 mm. The PE signal generated by PVDF sensor was analyzed by using a lock-in amplifier (SR-530) to produce the PE amplitude and phase. The electromagnetic noise was reduced by eliminating all the ground loops via proper grounding.

The typical PE signal was measured with respect to time to investigate the steady state of the signal. The sensitivity of the back PPE technique was tested by maintaining the cavity length at about 100 µm, and the PE signal was recorded over 300 s. The experiment was carried out with
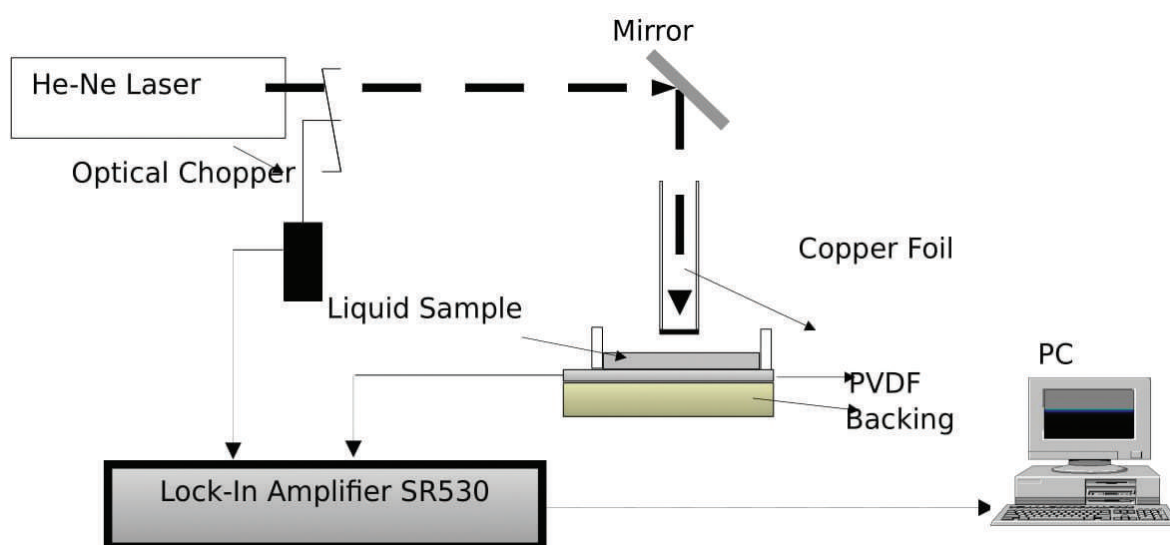

Figure 5. Schematic diagram of back PPE configuration [51].

a single drop of DW. In **Figure 6**, it can be observed that the PE signal was quite stable around 1.49×10^{-3} V with a standard deviation of 5.12×10^{-5} V.

A frequency scan was carried out as it was important to choose the optimal value of frequency for thermophysical measurements of nanofluids. **Figure 7** displays the frequency behaviour of the signal amplitude obtained from the distilled water as a reference sample with known thermal properties. It can be observed that at frequencies above 7 Hz, the effect of thermally thick regime become obvious. The amplitude of the PE signal of the sample decreased exponentially to zero with increasing modulation of the frequency in the thermally thick regime. Therefore, the frequency range between 7 and 30 Hz was used for the frequency scan, which is shown in **Figure 5**. The noise level in the present setup was about 75 μV. The ln(amplitude) of the PE signal as a function of $f^{1/2}$ in this useful frequency range was linear. The thermal diffusivity was calculated from the slope of the linear part of the logarithmic amplitude of the signal curves by using Equation (6b).

3.2.2. Front photopyroelectric configuration

In the new section design, a simplified front PPE configuration was setup using the similar PE sensor. The metalized PVDF sensor was used as an optically opaque sensor and in a thermally thick regime for both the sensor and sample, instead of a very thick sensor (usually $LiTaO_3$) in
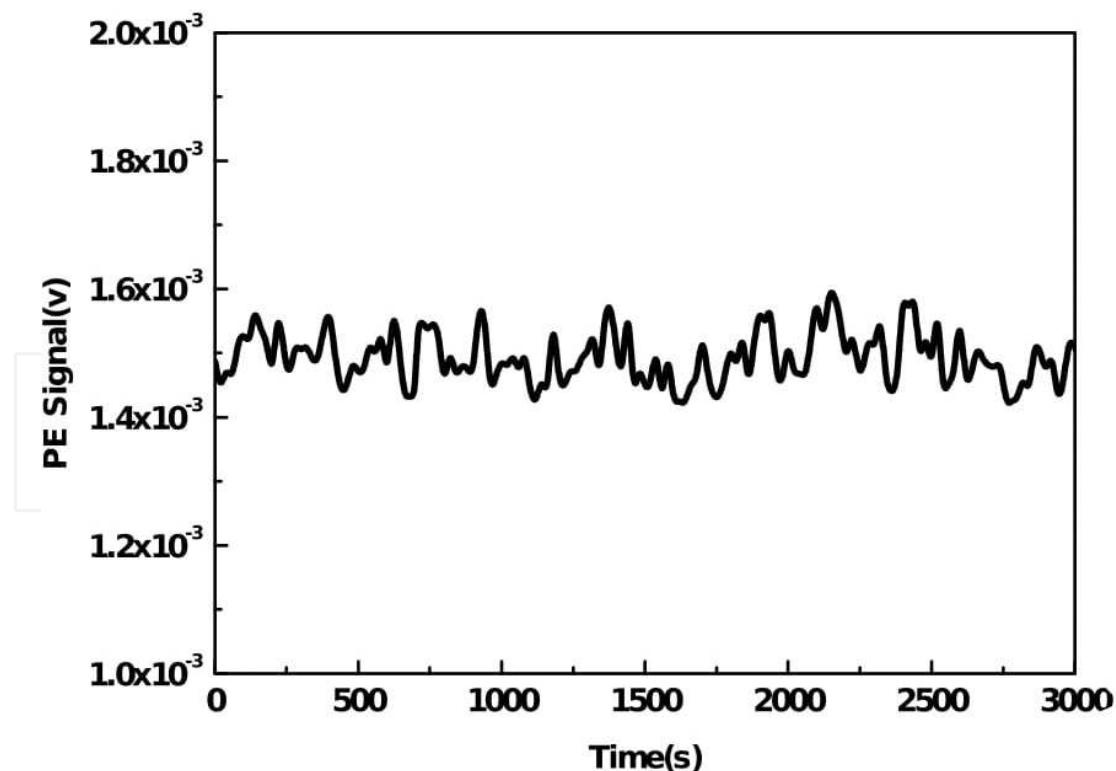
Figure 6. PVDF signals recorded versus time for distilled water; the baseline is a steady-state signal in various times.
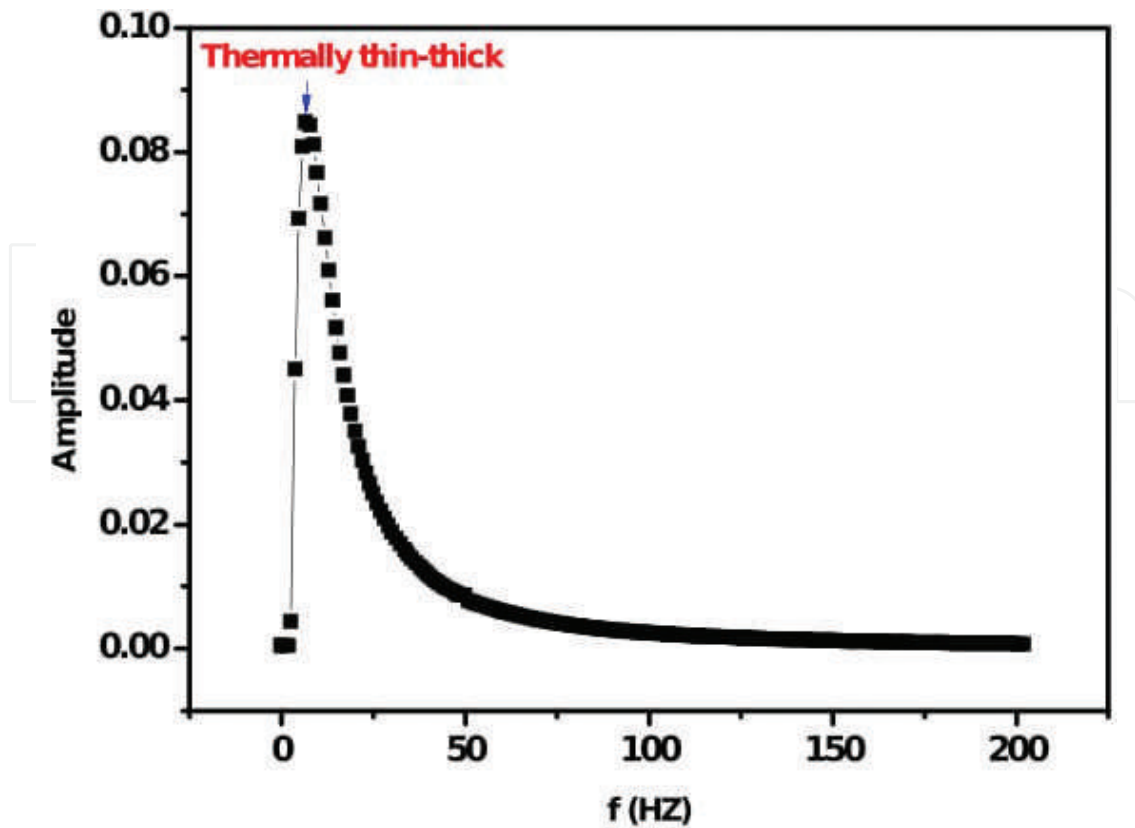
Figure 7. Frequency behaviour of the amplitude of signal obtained from the distilled water [52].

the conventional front PPE configuration [53, 57]. The radiation from the similar He-Ne laser was modulated by the mechanical chopper, and the signal from the PVDF sensor was processed with the lock-in amplifier. The liquid sample was simply filled into a plastic ring and glued on the rear side of the sensor, and the overall thickness was about 1 mm. As the sample thickness decreased, the contribution from the reflected TW power increased. A schematic view of the experimental setup of the front PPE is presented in **Figure 8**. The scan was performed in thermally thick conditions in a frequency range of 7 to 30Hz with 1Hz steps. The S/N ratio of the experiment was more than 750. The LabVIEW software was used to capture the amplitude and phase data, and the data were analyzed using Microcal Origin 8. The following procedure describes the steps from the recorded experimental data up to obtaining thermal effusivity of the nanofluid by fitting the normalized phase of the PE signal versus frequency scan to obtain thermal effusivity (e_p or e_s).

Figure 9 (a–b) displays the frequency behaviour of the normalized amplitude and phase of signal obtained from DW as a reference sample of known thermal effusivity, $1600 Ws^{1/2}m^{-2}K^{-1}$ [53], to determine the thermal effusivity of the PVDF sensor. In **Figure 9 (a–b)**, the frequency range between 7 and 30 Hz was the best choice for fitting to find the parameters. However, here, the phase was used instead of the amplitude because it produced more accurate results as it did not change with source intensity fluctuations.
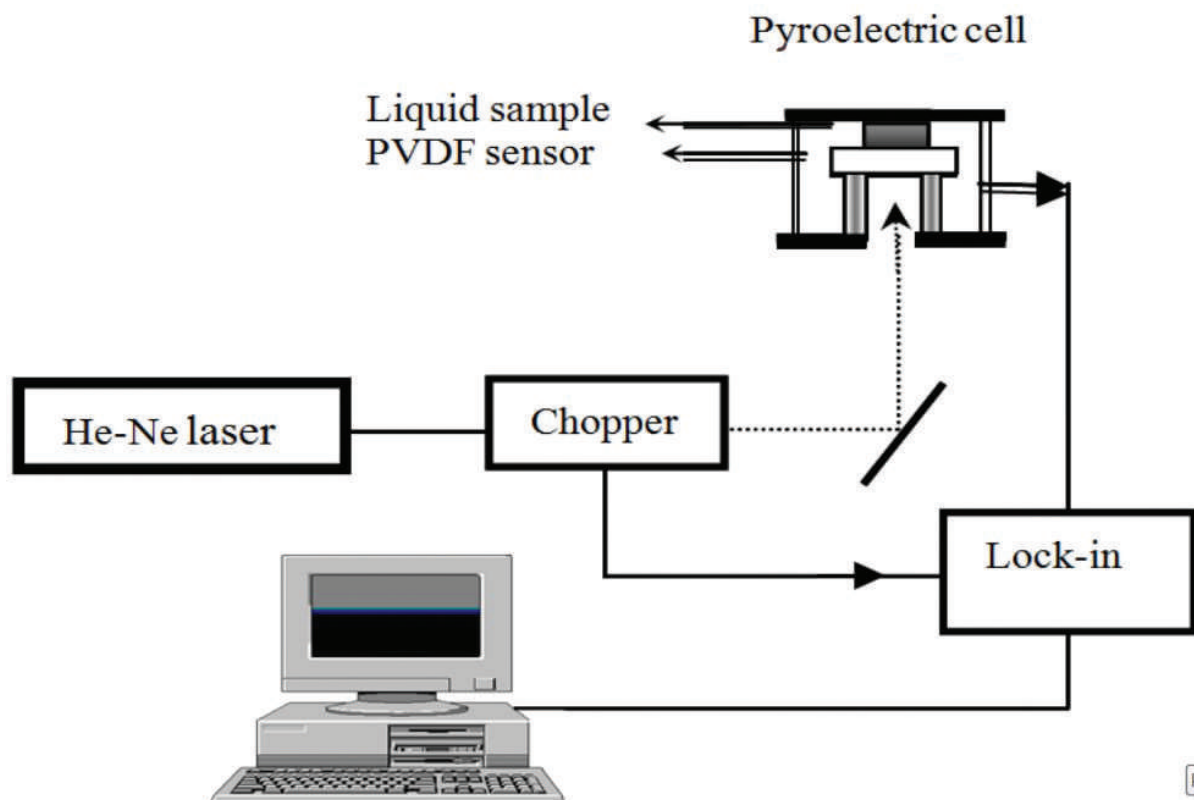
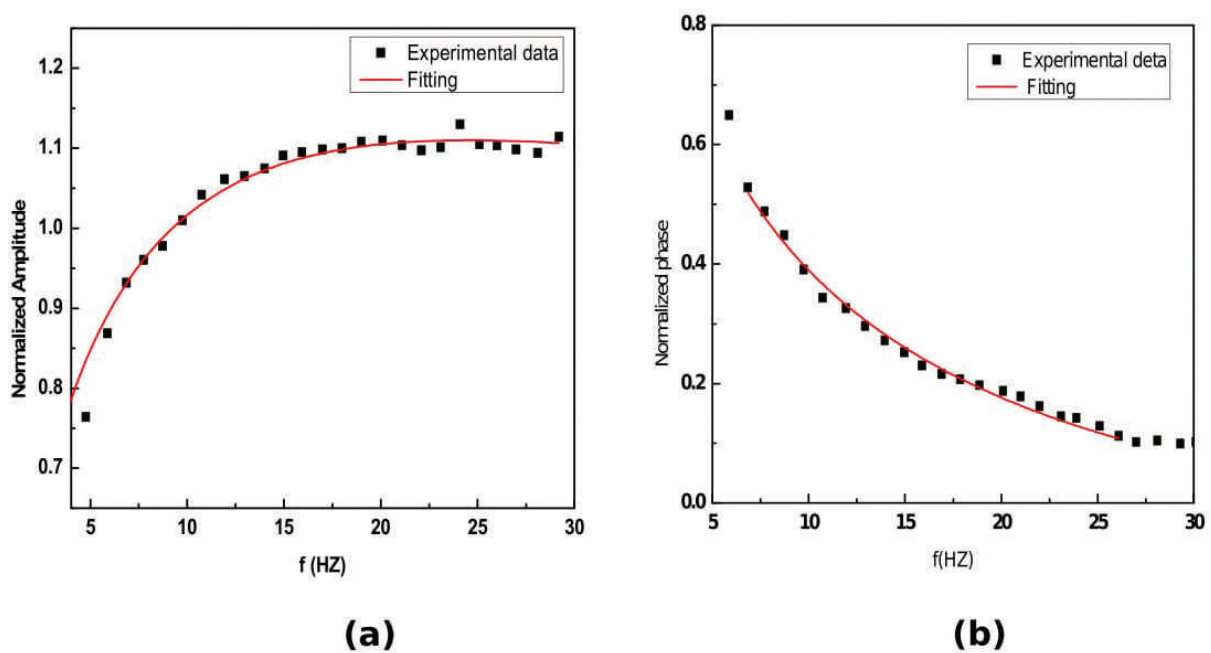**Figure 8.** Schematic view of experimental setup of front PPE configuration [54].

Figure 9. Frequency behaviour of the normalized (a) amplitude and (b) phase measured for the PVDF sensor with water as substrate. Solid lines are the best fit of amplitude to Equation (10b) and phase to Equation (10a), respectively [54].

4. Results and discussion

4.1. Effect of ultrasonication on the thermal diffusivity of Al2O3 nanofluids

4.1.1. Sample preparation and characterization

In the study, the influence of ultrasonication on the thermal diffusivity of low concentration of Al_2O_3 nanofluids in two sizes of NPs, size A (11 nm) and size B (30 nm) in water were investigated. Each nanofluid sample 0.125%, 0.25% and 0.5 wt% was dissolved in DW and magnetically stirred vigorously until a clear solution was observed after about 1 h. Two different ultrasonic systems were chosen to disperse the NPs in DW for 30 min using the bath sonicator, called sample B, or the probe sonicator, called sample P, respectively. The total
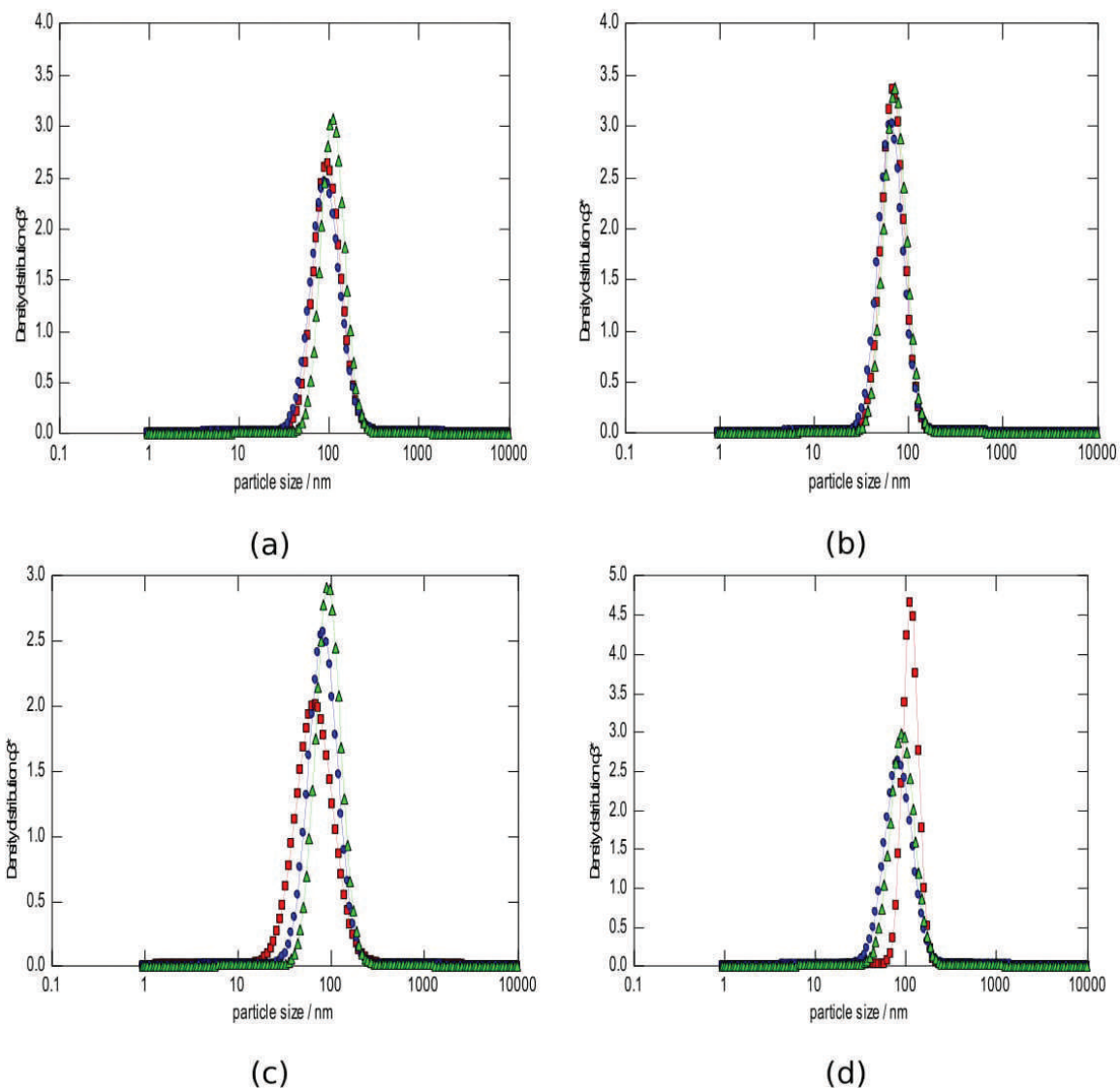

Figure 10. Particle size distributions determined using the Nanophox analyzer of Al_2O_3 particles in the nanofluids after three measurements at 15 min intervals, for NPs of size A (a,b) and B (c,d) prepared using the bath (a,c) and probe (b,d) sonicators. PDS just after sonication (□), after 15 min (◎) and after 30 min (Δ) [51].

amount of energy delivered to the sample was constant for both sonicators. After each ultrasonication, the mean particle size was measured using the Nanophox particle size analyzer (Sympatec GmbH, D-38678), and an average was taken from at least three measurements. The morphology of the alumina clusters was characterized by TEM.

Figure 10 shows the particle size distribution (PSD) and the hydrodynamic diameters of the Al_2O_3 NPs in the nanofluids. It can be seen that the NP agglomerates were only slightly broken up by the bath sonicator (**Figure 10 a, c**); however, the large agglomerates were completely broken down by the probe sonicator (**Figure 10 b, d**). The smallest mean PSD was recorded for samples with small particle size, A, prepared using probe sonication. There was no significant change in the mean particle size for the three measurements (**Figure 10 b**). However, in all cases, the NPs agglomerated in water were not completely broken up using sonication, whether by using the bath or probe sonicators.

The UV-Vis absorption spectra of the Al_2O_3 NPs prepared in DW, using bath- and probe-type ultrasonicator for the dispersion of the particles, are shown in **Figure 11**. The increase of absorption behaviour of the sample prepared using the ultrasonic probe could be attributed
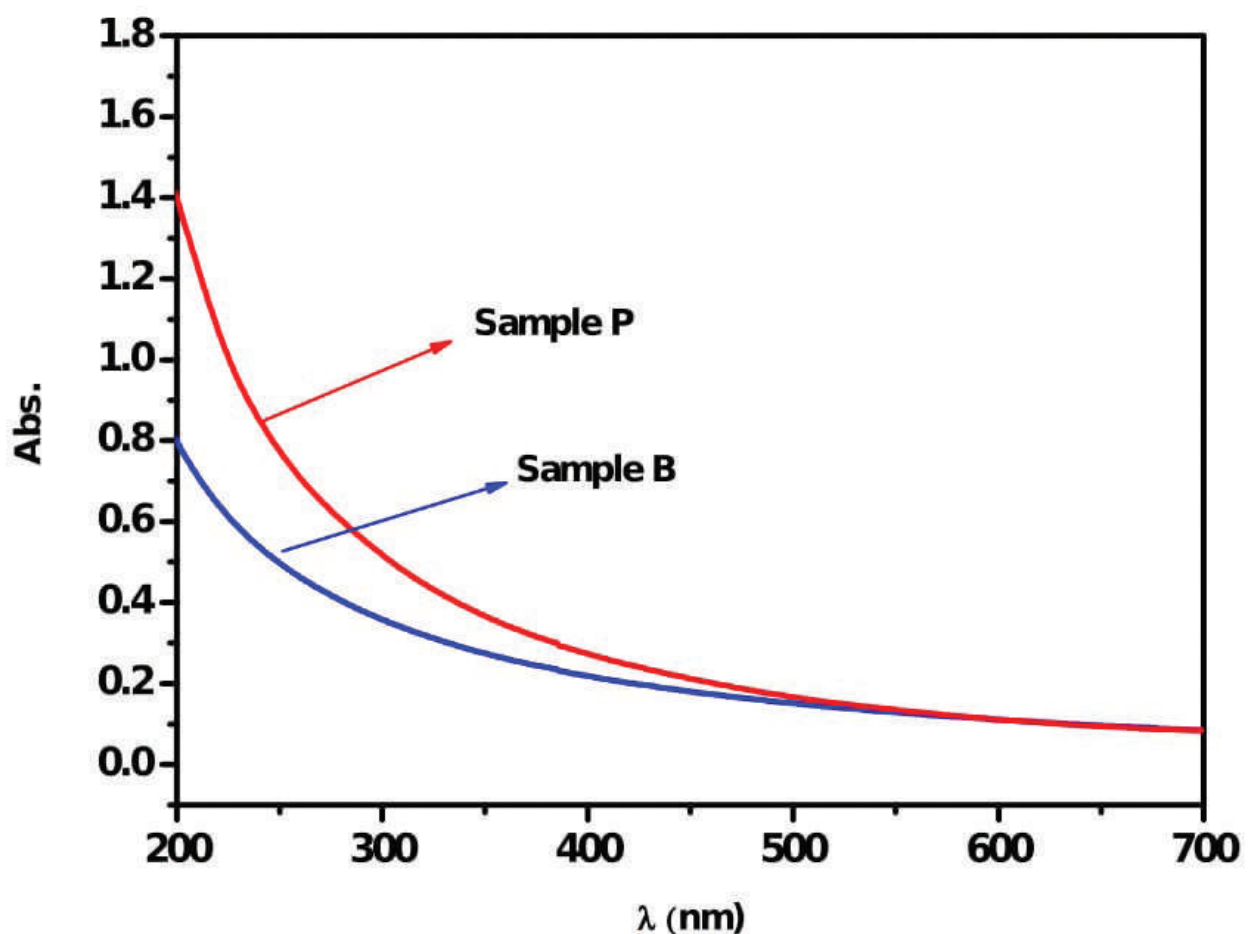

Figure 11. UV-Vis absorption spectra of the Al_2O_3 nanofluids, in the treatment by bath (sample B) and probe (sample P) sonication, respectively.

to the increase in quantity of Al_2O_3 NPs assembled within the fluid, as proven by the Nanophox results. This indicated that for the sample prepared using the ultrasonic probe, the absorption of nanofluids was at a maximum; therefore, the stability of the nanofluid was high, and the agglomeration between particles was reduced [50].

The effect of ultrasonic irradiation on the synthesized Al_2O_3 nanofluids was analyzed by TEM. **Figure 12** shows the TEM images of Al_2O_3 NPs of two sizes A and B prepared in DW without sonication (a,b) and prepared using the bath (c,d) and the probe (e,f) sonicators, for NPs of size A (a,c,e) and B (b,d,f), respectively. It can be seen that most of the NPs were spherical and were connected to each other to form a porous structure. The size of the NPs was well distributed in both ultrasonic sonicators, as shown in **Figure 12** (c,d). However, the probe sonicator was more effective in reducing particle sizes to below 100 nm, as shown in **Figure 12** (e,f). As previously mentioned, in all nanofluids, the measured particle sizes were larger than the nominal particle sizes claimed by the vendor. This indicated that the oxide NPs agglomerated in water and the hard aggregates could not be broken down into individual NPs under these operating conditions or even with very high-energy input [18].

4.1.2. Enhancement of thermal diffusivity

Before measuring thermal diffusivity of the nanofluids, the PPE setup was tested with DW as the base fluid. The recorded α value was $(1.431 \pm 0.030) \times 10^{-3}$ cm^2/s, which differed by less than 2% from the values reported in literature [49]. The thermal diffusivity of the Al_2O_3 nanofluids prepared using different sonication techniques at different concentrations of NPs of sizes A and B was obtained. **Figure 13** shows the typical behaviour of the (a) amplitude of the PE signal versus the frequency and (b) the plot of ln(amplitude) of PE signal versus square root of frequency. The thermal diffusivity can be calculated from the fitting slope of the linear part of the signal curves. The thermal diffusivity data are summarized in **Tables 2** and **3**. The data indicated that the thermal diffusivity of the Al_2O_3 nanofluids was higher than that of water.

The data also proved that the thermal diffusivity enhancement was greater for the smaller-sized NPs. This was because smaller particles have larger surface area (the heat transfer area), thus increasing the thermal diffusivity [55]. Hence, smaller particles helped form a stable nanofluid, and the probe sonicator had a substantial effect on the thermal diffusivity. At a given particle concentration, the thermal diffusivity enhancement was greater for the probe than the bath sonicator. This was because the NPs were more widely dispersed in water through probe sonication, generating a larger NP surface area and thus increasing the thermal diffusivity. The beneficial effect of using the probe sonicator on the thermal diffusivity of Al_2O_3 nanofluids was more pronounced at high particle concentrations and small particle sizes. For example, the greatest enhancement of thermal diffusivity of 6% was achieved for the probe sonicator with NPs of size A at a concentration of 0.5 wt%. The smallest enhancement was about ≈1% for NPs of size B at 0.125 wt% with the bath sonicator. These findings are possibly attributable to the rapid particle clustering at a high concentration, which necessitates using a more powerful sonication tool to break up large agglomerates into smaller-sized particles.
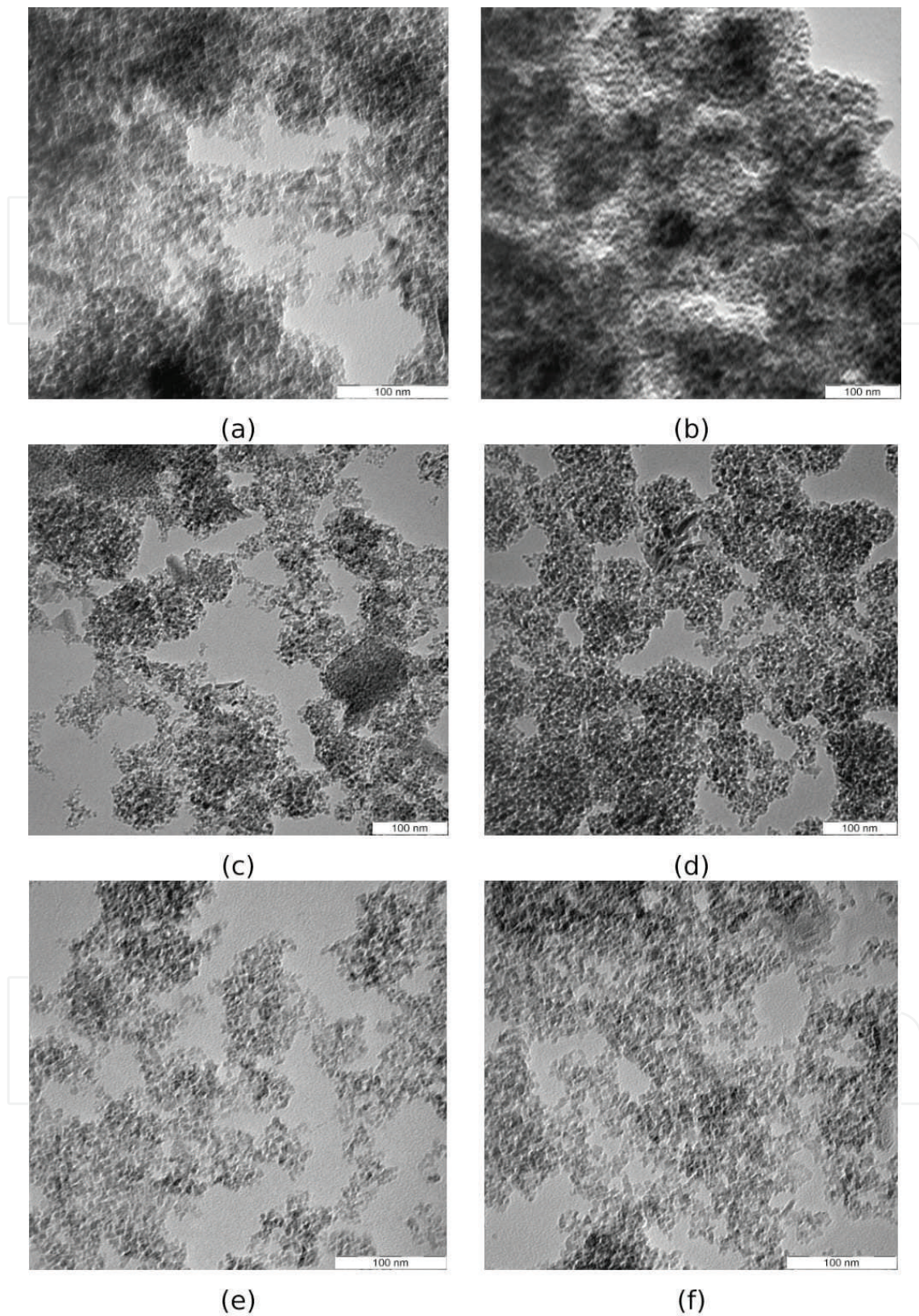
Figure 12. TEM images of Al_2O_3 NPs prepared in DW without (a,b) and with (c,d) the bath sonicator and (e,f) probe sonicators, for NPs of size 11 nm (a,c,e) and 30 nm (b,d,f) [51].
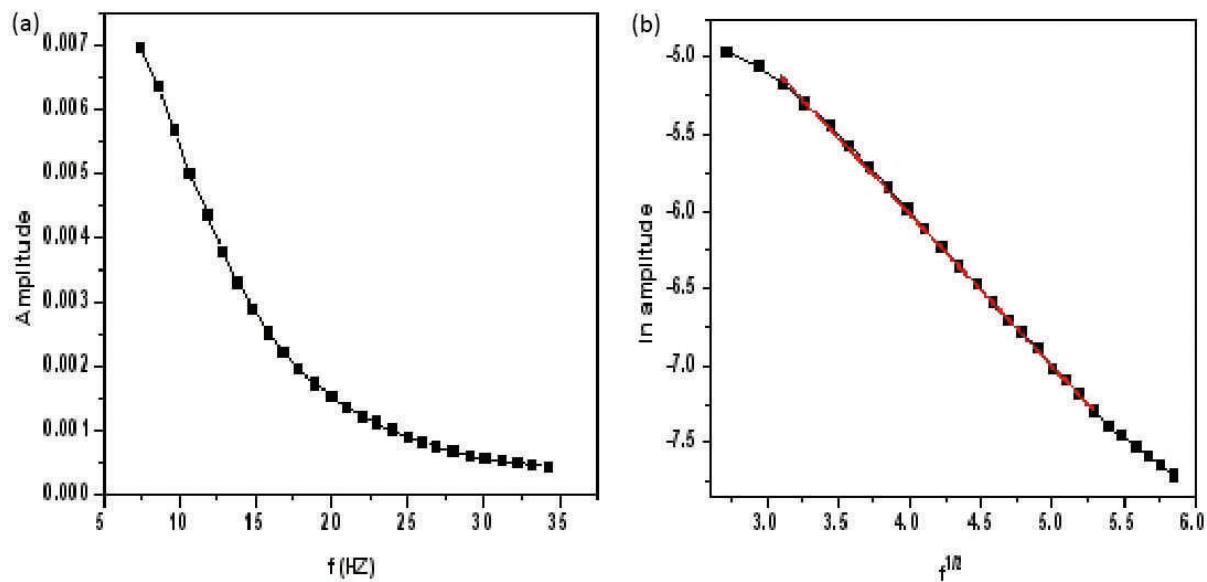
Figure 13. (a) Amplitude of the PE signal as a function of the chopping frequency f and (b) natural log of the amplitude of the PE signal as a function of the square root of the chopping frequency and its fitting by using Equation (6b), for one of the samples [51].

Concentration wt%	Bath		Probe	
	Thermal diffusivity $(cm^2/s)10^{-3}$	Thermal diffusivity enhancement %	Thermal diffusivity $(cm^2/s)10^{-3}$	Thermal diffusivity enhancement %
0.125	1.476 ± 0.002	3.1	1.482 ± 0.004	3.5
0.25	1.483 ± 0.003	3.5	1.494 ± 0.002	4.3
0.5	1.492 ± 0.004	4.2	1.515 ± 0.003	5.8

Table 2. Thermal diffusivity of Al_2O_3 nanofluids, NP type A (11 nm), prepared by using different sonication techniques at different NP concentrations [51].

Concentration wt%	Bath		Probe	
	Thermal diffusivity $(cm^2/s)10^{-3}$	Thermal diffusivity enhancement %	Thermal diffusivity $(cm^2/s)10^{-3}$	Thermal diffusivity enhancement %
0.125	1.446 ± 0.003	0.9	1.448 ± 0.001	1.1
0.25	1.461 ± 0.002	2.1	1.473 ± 0.002	2.9
0.5	1.478 ± 0.004	3.2	1.498 ± 0.003	4.6

Table 3. Thermal diffusivity of Al_2O_3 nanofluids, NP type B (30 nm), prepared by using different sonication techniques at different NP concentrations [51].

4.2. Effect of base fluids on thermal effusivity of nanofluids

4.2.1. Sample preparation and characterization

The thermal effusivity of Al_2O_3 (11 nm) and CuO (50 nm) NPs dispersed in three different base fluids, DW, EG and olive oil, in the presence of the stabilizer polyvinylpyrrolidone (PVP) was investigated. In each nanofluid, sample 0.125 wt% was dissolved in each base fluid and magnetically stirred vigorously until a clear solution were observed after about 1 h. The solution was then sonicated by probe sonicator for 30 min to ensure a uniform dispersion of NPs in the fluids. TEM was employed to obtain the morphology of the CuO and Al_2O_3 particles and to determine the average particle size.

Figure 14 shows the TEM images and their corresponding size distributions of (a) CuO and (b) Al_2O_3 nanofluids prepared in water. It can be seen that most of the NPs were well dispersed and some agglomerates were present. The CuO and Al_2O_3 NP sizes were about 52.3 ± 4.2 nm and 7.5 ± 2.5 nm, respectively. These commercial NPs determined from TEM images were
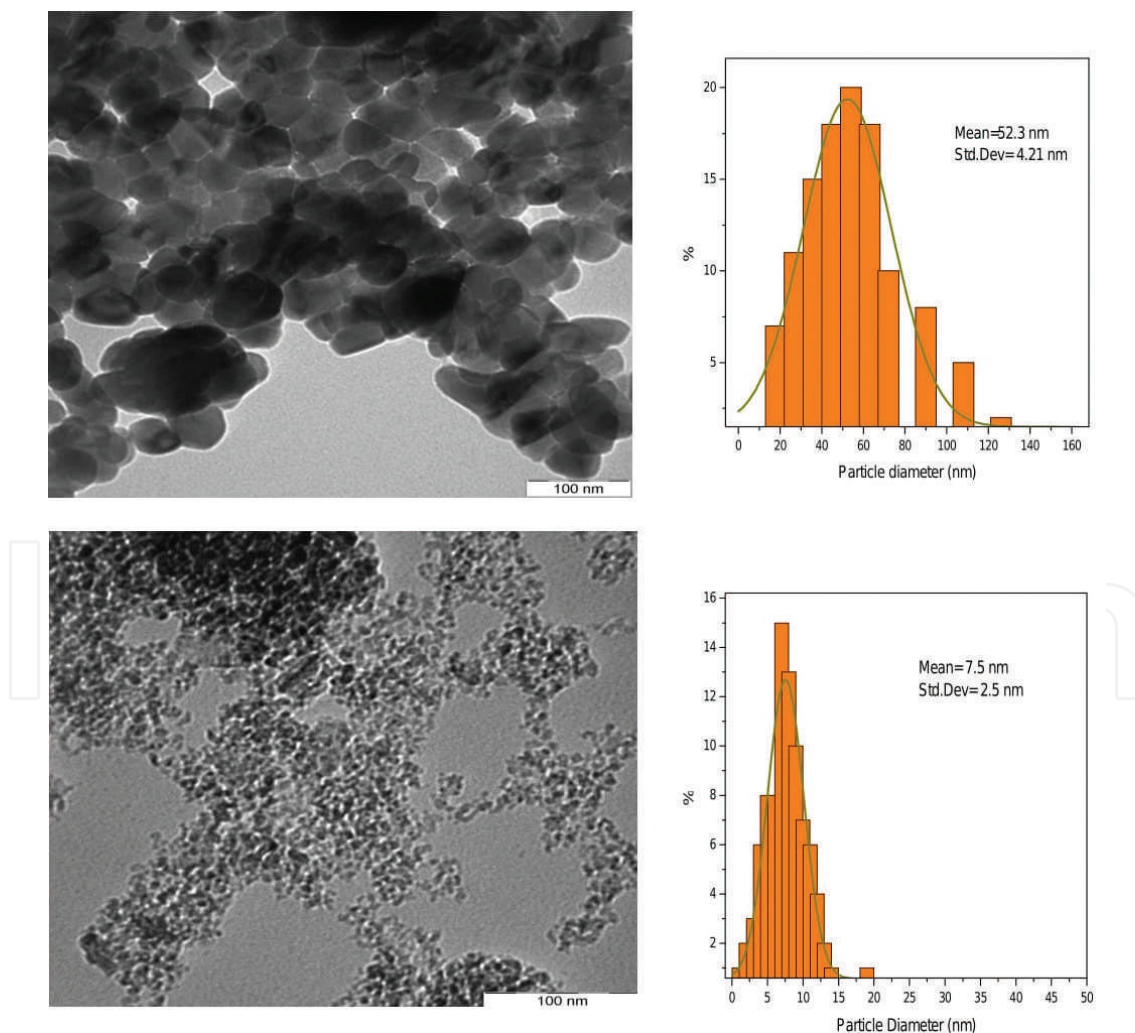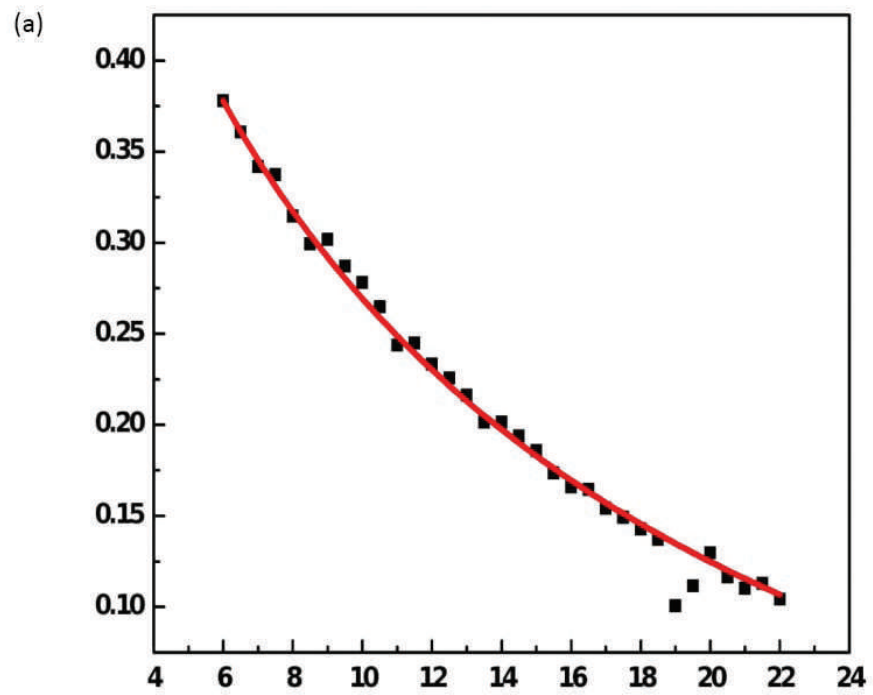

Figure 14. TEM images and their size distributions of (a) CuO particles and (b) Al_2O_3 nanofluids prepared in water [56].
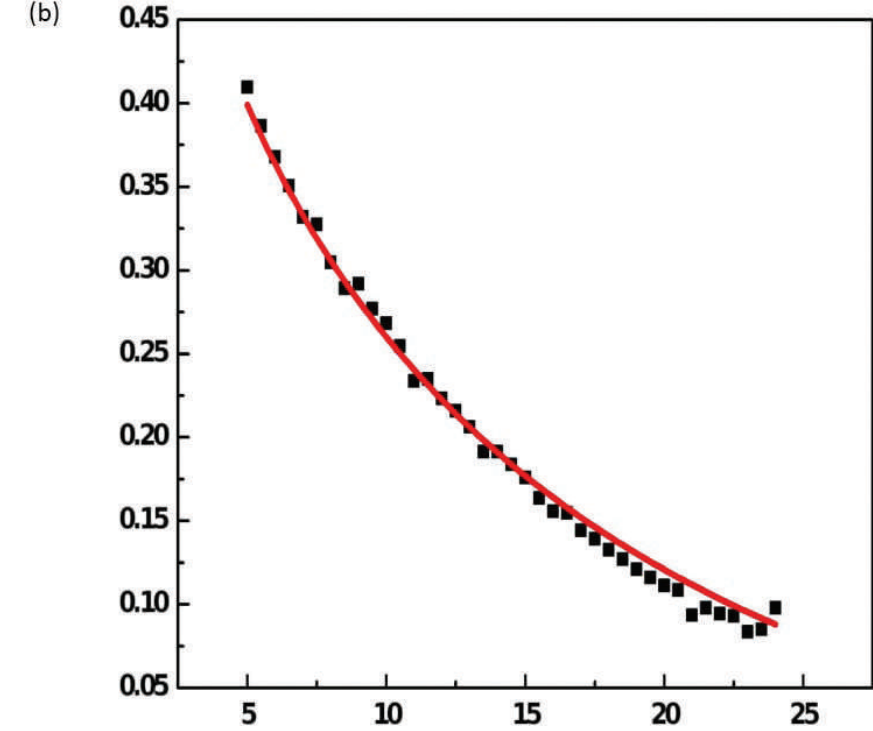
±

(a)

±

(b)

Figure 15. The experimental data and the best fit of the PE normalized phase versus modulation frequency in (a) Al_2O_3/olive oil and (b) CuO/olive oil, obtained by using Equation (10a) [56].

slightly different from those reported by the vendors. This indicated that some of particles in each sample were aggregated with some uniform size distribution as reported by them.

4.2.2. Thermal effusivity measurements

Figure 15 shows the PE-normalized phase versus modulation frequency in (a) Al_2O_3/olive oil and (b) CuO/olive oil. It was observed that from this fit the values of A from Equation (9) were obtained at (1.112 ± 0.005) and (1.175 ± 0.006), corresponding to the values of thermal effusivity of Al_2O_3/olive oil $(0.614 \pm 0.003) \times 10^3$ $Ws^{1/2}m^{-2}K^{-1}$ and CuO/olive oil $(0.697 \pm 0.003) \times 10^3$ $Ws^{1/2}m^{-2}K^{-1}$, respectively, obtained by using Equation (10a). The values of thermal effusivity measured for all nanofluids and their comparison with pure solvents are summarized in **Table 3** and **Figure 16**. The comparisons indicated that the thermal effusivity of the various base fluids mixed with NPs in the presence of PVP were reduced as compared to pure fluids, possibly due to the effect of the surfactant that inhibited the thermal effusivity of the nanofluids [56]. The results also showed that the base fluids had more influence on effusivity than the NPs. The relative standard deviation for measuring the thermal effusivity of
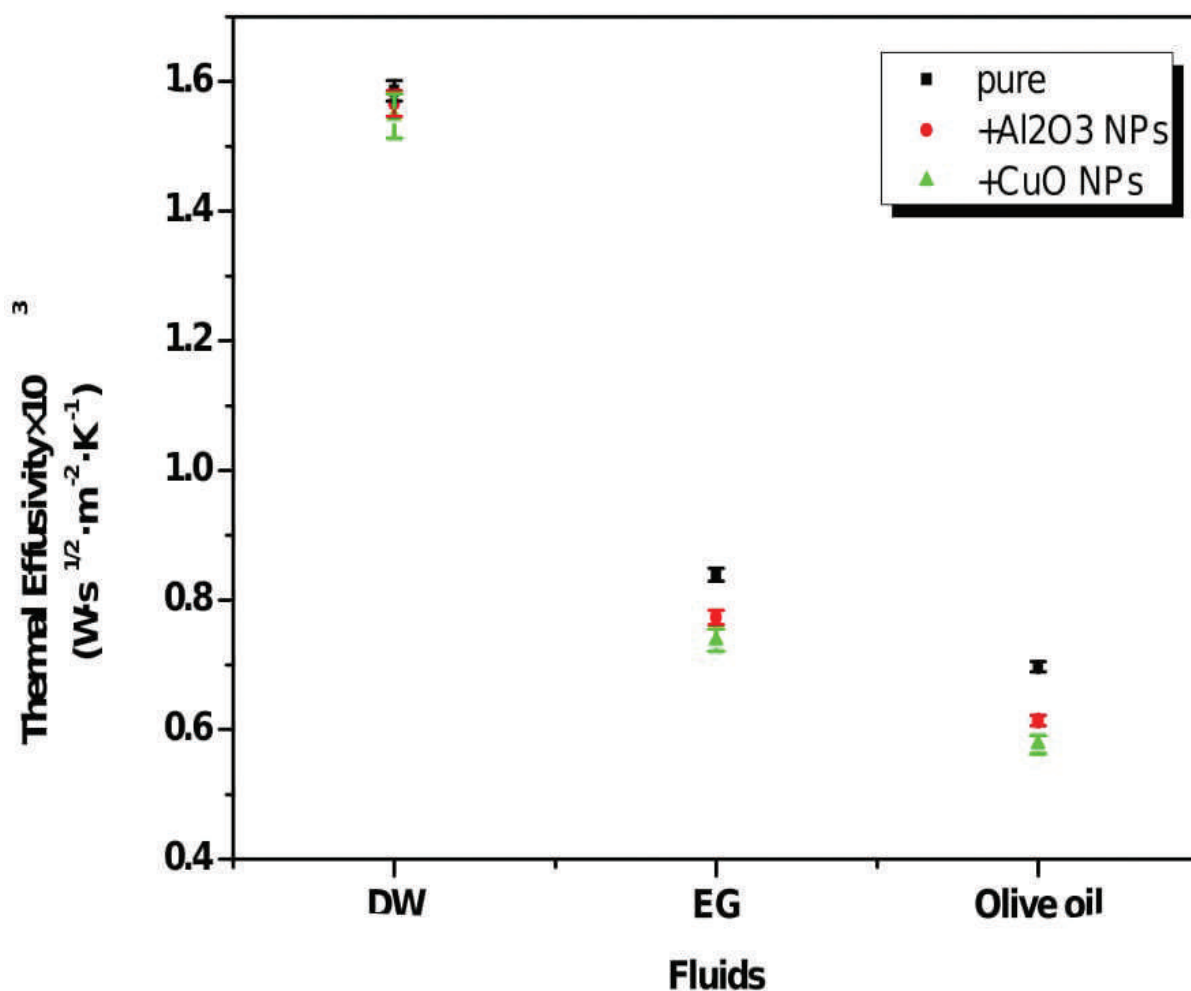

Figure 16. Thermal effusivity of Al_2O_3 and CuO nanofluids with (DW, EG and olive oil) and their pure solvents [56].

nanofluids was below 2%, as shown in **Table 4**. Therefore, the front PPE technique is a promising high-accuracy alternative for this measurement.

NPs	Base fluid	Fitting parameter(A)	Thermal effusivity × 10^3 (Ws$^{1/2}$ m^{-2} K^{-1}) measurement	Relative error%	Thermal effusivity × 10^3 (Ws$^{1/2}$ m^{-2} K^{-1}) literature
Al$_2$O$_3$	Water	1.523 ± 0.014	1.566 ± 0.015	0.95	–
Al$_2$O$_3$	EG	1.223 ± 0.009	0.773 ± 0.006	0.77	–
Al$_2$O$_3$	Olive	1.112 ± 0.005	0.614 ± 0.003	0.48	–
CuO	Water	1.519 ± 0.028	1.547 ± 0.029	1.87	–
CuO	EG	1.202 ± 0.021	0.738 ± 0.012	1.75	–
CuO	Olive	1.081 ± 0.018	0.577 ± 0.009	1.56	–
–	Water	1.528 ± 0.011	1.586 ± 0.011	0.69	1.579 [10]
–	EG	1.263 ± 0.008	0.839 ± 0.005	0.59	0.810 [11]
–	Olive	1.175 ± 0.006	0.697 ± 0.003	0.43	0.621 [11]

Table 4. Experimental thermal effusivity of Al$_2$O$_3$ and CuO nanofluids and their pure solvents and their literature values [56].

5. Conclusions

The PPE technique is a sensitive method to measure the thermal properties of nanofluids in small volumes. Following this, the back PPE configuration was used to obtain the influence of ultrasonic irradiation modes (either bath or probe sonication) such as the cluster size of Al$_2$O$_3$ nanofluids in low concentrations on the thermal diffusivity. The ultrasonic bath proved to be almost ineffective in size reduction, as most of the Al$_2$O$_3$ particles were spherical and were connected to each other to form a porous structure ranging in size from 1 μm to larger, and the probe sonication effectively reduced the particle size to below 100 nm. This showed that the oxide NPs in water were agglomerated and some hard aggregates could not be broken into individual NPs under these operating conditions or even at very high-energy inputs. The proposed front PPE technique, with a metalized PVDF sensor in a thermally thick regime, was applied to measure thermal effusivity by utilizing the phase signal of nanofluids that contained Al$_2$O$_3$ and CuO NPs dispersed in different solvents, water, ethylene glycol and olive oil. As expected, the relative standard deviation of this measurement, 2%, confirmed that this method was also suitable for measuring the thermal effusivity of nanofluid with a high degree of accuracy.

Abbreviations and Nomenclature

Q_o TW source intensity
ω Angular frequency of modulated light
f Modulation frequency

ε_0	Permittivity constant of vacuum
T_{jk}	TW transmission coefficient
R_{jk}	TW reflection coefficient
σ	Complex TW diffusion
μ	Thermal diffusion length
k	Thermal conductivity
α	Thermal diffusivity
e	Thermal effusivity
L_s	Sample thickness
DW	Deionized water
NPs	Nanoparticles
PPE	Photopyroelectric
PE	Pyroelectric
PVDF	Polyvinylidene fluoride
PSD	Particle size distribution
SNR	Signal-to-noise ratio
TW	Thermal wave
TWC	Thermal-wave cavity
EG	Ethylene glycol

Author details

Monir Noroozi* and Azmi Zakaria

*Address all correspondence to: monir.noroozi@gmail.com

Physics Department, Faculty of Science, Universiti Putra Malaysia, Malaysia

References

[1] Murshed SMS, Leong KC, Yang C. Thermophysical and electrokinetic properties of nanofluids—a critical review. Applied Thermal Engineering, 2008; **28**: 2109–2125.

[2] Masuda H, Ebata A, Teramae K, Hishinuma N. Alteration of thermal conductivity and viscosity of liquid by dispersing ultra-fine particles [dispersion of Al_2O_3, SiO_2 and TiO_2 ultra-fine particles. Netsu Bussei. 1993; **4**: 227–233

[3] Choi SUS, Eastman JA. Enhancing thermal conductivity of fluids with nanoparticles. osti. gov, International mechanical engineering congress and exhibition, San Francisco, CA (United States), 1995; 12–17 Nov 1995

[4] Wang XQ, Mujumdar AS. Heat transfer characteristics of nanofluids: a review. International Journal of Thermal Sciences 2007; **46**: 1–19.

[5] Sheikholeslami M, Hayat T, Alsaedi A. MHD free convection of Al_2O_3–water nanofluid considering thermal radiation: a numerical study. International Journal of Heat and Mass Transfer, 2016; **96**: 513–524.

[6] Eastman JA, Choi SUS, Li S, Yu W, & Thompson LJ. Anomalously increased effective thermal conductivities of ethylene glycol-based nanofluids containing copper nanoparticles. Applied Physics Letters. 2001; **78**: 718–720.

[7] Evans W, Prasher R, Fish J, Meakin P, Phelan P, Keblinski P. Effect of aggregation and interfacial thermal resistance on thermal conductivity of nanocomposites and colloidal nanofluids. International Journal of Heat and Mass Transfer. 2008; **51**: 1431–1438.

[8] Sheikholeslami M, Ellahi R. Three dimensional mesoscopic simulation of magnetic field effect on natural convection of nanofluid. International Journal of Heat and Mass Transfer, 2015;**89**: 799–808.

[9] Murshed SMS, Leong KC, Yang C. Determination of the effective thermal diffusivity of nanofluids by the double hot-wire technique. Journal of Physics D: Applied Physics 2006; **39**: 5316.

[10] Shen J, and Mandelis A. Thermal-wave resonator cavity. Review of Scientific Instruments 1995; **66**: 4999–5005

[11] Chirtoc M, Mihilescu G. Theory of the photopyroelectric method for investigation of optical and thermal materials properties. Physical Review B 1989; **40**: 9606–9617.

[12] Kwan CH, Matvienko A, Mandelis A. Optimally accurate thermal-wave cavity photopyroelectric measurements of pressure-dependent thermophysical properties of air: theory and experiments. Review of Scientific Instruments 2007; **78**: 104902–104910.

[13] Chirtoc M, Bentefour EH, Glorieux C., Thoen J. Development of the front-detection photopyroelectric (FPPE) configuration for thermophysical study of glass-forming liquids. Thermochimica Acta. 2001; **377**: 105–112.

[14] Dădârlat D, Neamtu C. Detection of molecular associations in liquids by photopyroelectric measurements of thermal effusivity. Measurement Science and Technology 2006; **17**: 3250.

[15] Longuemart S, Quiroz AG, Dadarlat D, Sahraoui AH, Kolinsky C, Buisine JM. An application of the front photopyroelectric technique for measuring the thermal effusivity of some foods. Instrumentation Science & Technology 2002; **30**: 157–165.

[16] Wei Y, Xie H. A review on nanofluids: preparation, stability mechanisms, and applications. Journal of Nanomaterials, 2012; **2012**: 17 pages

[17] Taylor R, Phelan P, Otanicar T, Adrian R, Prasher R. Nanofluid optical property characterization: towards efficient direct absorption solar collectors. Nanoscale Research Letters, 2011; **6**: 225.

[18] Nguyen VS, Rouxel D, Hadji R, Vincent B, Fort Y. Effect of ultrasonication and dispersion stability on the cluster size of alumina nanoscale particles in aqueous solutions. Ultrasonics Sonochemistry, 2011; **18**: 382–388.

[19] Dadarlat D, Longuemart S, Turcu R, Streza M, Vekas L, Hadj Sahraoui A. Photopyro-electric calorimetry of Fe_3O_4 magnetic nanofluids: effect of type of surfactant and magnetic field. International Journal of Thermophysics, 2014;**35**: 2032–2043.

[20] Nisha MR, Philip J. Dependence of particle size on the effective thermal diffusivity and conductivity of nanofluids: role of base fluid properties. Heat and Mass Transfer, 2012; **48**:1783–1790.

[21] Philip J, Nisha MR. Thermal diffusion in dilute nanofluids investigated by photothermal interferometry. Journal of Physics: Conference Series, 2010; **214**: 012035.

[22] López-Muñoz GA, Balderas-López JA, Ortega-Lopez J, Pescador-Rojas JA, Salazar JS. Thermal diffusivity measurement for urchin-like gold nanofluids with different solvents, sizes and concentrations/shapes. Nanoscale Research Letters, 2012; **7**: 1–7.

[23] Dadarlat D, Neamtu C, Streza M, Turcu R, Craciunescu I, Bica D, et al. High accuracy photopyroelectric investigation of dynamic thermal parameters of Fe_3O_4 and $CoFe_2O_4$ magnetic nanofluids. Journal of Nanoparticle Research, 2008; **10**: 1329–1336.

[24] Agresti F, Ferrario A, Boldrini S, Miozzo A, Montagner F, Barison S, et al. Temperature controlled photoacoustic device for thermal diffusivity measurements of liquids and nanofluids. Thermochimica Acta, 2015; **619**:48–52.

[25] Sánchez-Ramírez JF, Pérez JLJ, Orea AC, Fuentes RG, Bautista-Hernández A, Pal U. Thermal diffusivity of nanofluids containing Au/Pd bimetallic nanoparticles of different compositions. Journal of Nanoscience and Nanotechnology, 2006; **6**: 685–690

[26] Kumar BR, Basheer NS, Kurian A, George SD. Effect of particle size on the thermo-optic properties of gold nanofluids—a thermal lens study. AIP Conference Proceedings, 2014; **1576**: 118–121.

[27] Jiménez Pérez LJ, Gutierrez Fuentes R, Sanchez Ramirez FJ, Cruz-Orea A. Study of gold nanoparticles effect on thermal diffusivity of nanofluids based on various solvents by using thermal lens spectroscopy. The European Physical Journal Special Topics, 2008; **153**: 159–161.

[28] Gutierrez Fuentes R, Pescador Rojas JA, Jiménez-Pérez JL, Sanchez Ramirez JF, Cruz-Orea A, Mendoza-Alvarez J G. Study of thermal diffusivity of nanofluids with bimetallic nanoparticles with Au(core)/Ag(shell) structure. Applied Surface Science 2008; **255**: 781–783.

[29] Filippo A, Simona B, Simone B, Cesare P, Laura C, Laura F, et al. Tuning the thermal diffusivity of silver based nanofluids by controlling nanoparticle aggregation. Nanotechnology, 2013; **24**: 365601.

[30] Wang ZL, Tang DW, Liu S, Zheng XH, Araki N. Thermal-conductivity and thermal-diffusivity measurements of nanofluids by 3ω method and mechanism analysis of heat transport. International Journal of Thermophysics, 2007;**28**: 1255–1268.

[31] Faris Mohammed A, Yunus WMM. Study of the effect of volume fraction concentration and particle materials on thermal conductivity and thermal diffusivity of nanofluids. Japanese Journal of Applied Physics, 2011; **50**: 085201.

[32] Murshed SS, de Castro CN, Lourenço MJV, Lopes MM, Santos FJV. Experimental investigation of thermal conductivity and thermal diffusivity of ethylene glycol-based nanofluids. Proceedings of the International Conference on Mechanical Engineering 2011 (ICME2011), 18–20 December 2011, Dhaka, Bangladesh

[33] Rondino F, D'Amato R, Terranova G, Borsella E, Falconieri M. Thermal diffusivity enhancement in nanofluids based on pyrolytic titania nanopowders: importance of aggregate morphology. Journal of Raman Spectroscopy2014; **45**: 528–532

[34] Dadarlat D, Frandas A. Inverse photopyroelectric detection of phase transitions. Applied Physics A, 1993; **57**: 235–238.

[35] Balderas-López, JA, & Mandelis A. New photopyroelectric technique for precise measurements of the thermal effusivity of transparent liquids. International Journal of Thermophysics. 2003; **24**: 463–471

[36] Esquef IA, Siqueira APL, da Silva MG, Vargas H, Miranda LCM. Photothermal gas analyzer for simultaneous measurements of thermal diffusivity and thermal effusivity. Analytical Chemistry, 2006; **78**: 5218–5221

[37] Streza M, Pop MN, Kovacs K, Simon V, Longuemart S, Dadarlat D. Thermal effusivity investigations of solid materials by using the thermal-wave-resonator-cavity (TWRC) configuration. Theory and mathematical simulations. Laser Physics, 2009; **19**: 1340–1344.

[38] Balderas-López JA, Jaime-Fonseca MR, Díaz-Reyes J, Gómez-Gómez YM, Bautista-Ramírez ME, Muñoz-Diosdado A, et al. Photopyroelectric technique, in the thermally thin regime, for thermal effusivity measurements of liquids. Brazilian Journal of Physics, 2016; **46**: 105–110.

[39] Gutiérrez-Juárez G, Ivanov R, Pichardo-Molina JP, Vargas-Luna M, Alvarado-Gil JJ, & Camacho A. Metrological aspects of auto-normalized front photopyroelectric method to measure thermal effusivity in liquids. International Journal of Thermophysics 2008; **29**: 2102–2115.

[40] George NA, Vallabhan C P G, Nampoori VPN, George AK, Radhakrishnan P. Use of an open photoacoustic cell for the thermal characterisation of liquid crystals. Applied Physics B 2001; **73**: 145–149.

[41] De Albuquerque JE, Balogh DT, Faria RM. Quantitative depth profile study of polyaniline films by photothermal spectroscopies. Applied Physics A 2007; **86**: 395–401

[42] Coufal H and Mandelis A. Pyroelectric sensors for the photothermal analysis of condensed phases. Ferroelectrics 1991; **118**: 379–409

[43] Caerels J, Glorieux C, Thoen J. Absolute values of specific heat capacity and thermal conductivity of liquids from different modes of operation of a simple photopyroelectric setup. Review of Scientific Instruments 1998; **69**: 2452–2458.

[44] Delenclos S, Chirtoc M, Sahraoui AH, Kolinsky C, Buisine JM. Assessment of calibration procedures for accurate determination of thermal parameters of liquids and their

temperature dependence using the photopyroelectric method. Review of Scientific Instruments. 2002; **73**: 2773–2780.

[45] Longuemart S, Sahraoui AH, Dadarlat D, Daoudi A, Laux V, & Buisine JM. Investigations of the thermal parameters of ferroelectric liquid crystals using the pyroelectric effect in the S C * phase. Europhysics Letters (EPL). 2003; **63**: 453.

[46] Shen J, Mandelis A, and Helen T. Signal generation mechanisms, intracavity-gas thermal-diffusivity temperature dependence, and absolute infrared emissivity measurements in a thermal-wave resonant cavity. Review of Scientific Instruments 1997; **69**: 197–203

[47] Streza M, Dadarlat D, Socaciu C, Bele C, Dulf F, Simon V. Photopyroelectric detection of vegetable oils' adulteration. Food Biophysics 2009; **4**: 147–150.

[48] Matvienko A, Mandelis A. Theoretical analysis of PPE measurements in liquids using a thermal-wave cavity. The European Physical Journal Special Topics. 2008; **153**: 127–129.

[49] Balderas-Lopez JA, & Mandelis A. Simple, accurate, and precise measurements of thermal diffusivity in liquids using a thermal-wave cavity. Review of Scientific Instruments. 2001; **72**: 2649–2652.

[50] Veeradate P, Voranuch T, Piyapong A, Pichet L. Preparation and characterization of alumina nanoparticles in deionized water using laser ablation technique. Journal of Nanomaterials. 2012; **2012**:6 pages

[51] Noroozi M, Radiman S, & Zakaria A. Influence of sonication on the stability and thermal properties of Al_2O_3 nanofluids. Journal of Nanomaterials 2014; **2014**: 10.

[52] Noroozi M, Radiman S, Zakaria A. & Soltaninejad S. Fabrication, characterization, and thermal property evaluation of silver nanofluids. Nanoscale Research Letters 2014; **9**: 1–10.

[53] Dadarlat D & Neamtu C. High performance photopyroelectric calorimetry of liquids. Acta Chimica Slovenica 2009; **56**: 225–236.

[54] Noroozi M, Zakaria A, Husin MS, Moksin MM, Wahab ZA. Investigating thermal parameters of PVDF sensor in the front pyroelectric configuration. International Journal of Thermophysics 2013; **34**: 2136–2143.

[55] Zhu D, Li X, Wang N, Wang X., Gao J, Li H. Dispersion behavior and thermal conductivity characteristics of Al_2O_3–H_2O nanofluids. Current Applied Physics. 2009; **9**: 131–139.

[56] Noroozi M, Zakaria A, Moksin M.M, Wahab ZA. An Investigation on the thermal effusivity of nanofluids containing Al_2O_3 and CuO nanoparticles. International Journal of Molecular Sciences 2012; **13**: 10350–10358.

[57] Menon PC, Rajesh RN, Glorieux C. High accuracy, self-calibrating photopyroelectric device for the absolute determination of thermal conductivity and thermal effusivity of liquids. Review of Scientific Instruments, 2009: **80**: 054904–054909.